A&A 518, A45 (2010)
DOI: 10.1051/0004-6361/201014510
© ESO 2010

Astronomy & Astrophysics

The CO luminosity and CO-H_2 conversion factor of diffuse ISM: does CO emission trace dense molecular gas?⋆

H. S. Liszt[1], J. Pety[2,3], and R. Lucas[4]

[1] National Radio Astronomy Observatory, 520 Edgemont Road, VA 22903-2475 Charlottesville, USA
e-mail: hliszt@nrao.edu
[2] Institut de Radioastronomie Millimétrique, 300 rue de la Piscine, 38406 Saint Martin d'Hères, France
[3] Obs. de Paris, 61 av. de l'Observatoire, 75014 Paris, France
[4] Al-MA, Avda. Apoquindo 3846 Piso 19, Edificio Alsacia, Las Condes, Santiago, Chile

Received 26 March 2010 / Accepted 8 May 2010

ABSTRACT

Aims. We wish to separate and quantify the CO luminosity and CO-H_2 conversion factor applicable to diffuse but partially-molecular ISM when H_2 and CO are present but C^+ is the dominant form of gas-phase carbon.
Methods. We discuss galactic lines of sight observed in HI, HCO^+ and CO where CO emission is present but the intervening clouds are diffuse (locally $A_V \lesssim 1$ mag) with relatively small CO column densities $N_{CO} \lesssim 2 \times 10^{16}$ cm^{-2}. We separate the atomic and molecular fractions statistically using E_{B-V} as a gauge of the total gas column density and compare N_{H_2} to the observed CO brightness.
Results. Although there are H_2-bearing regions where CO emission is too faint to be detected, the mean ratio of integrated CO brightness to N_{H_2} for diffuse ISM does not differ from the usual value of 1 K km s^{-1} of integrated CO brightness per 2×10^{20} H_2 cm^{-2}. Moreover, the luminosity of diffuse CO viewed perpendicular to the galactic plane is 2/3 that seen at the Solar galactic radius in surveys of CO emission near the galactic plane.
Conclusions. Commonality of the CO-H_2 conversion factors in diffuse and dark clouds can be understood from considerations of radiative transfer and CO chemistry. There is unavoidable confusion between CO emission from diffuse and dark gas and misattribution of CO emission from diffuse to dark or giant molecular clouds. The character of the ISM is different from what has been believed if CO and H_2 that have been attributed to molecular clouds on the verge of star formation are actually in more tenuous, gravitationally-unbound diffuse gas.

Key words. ISM: molecules – ISM: clouds

1. Introduction

It is a truism that sky maps of CO emission are understood as uniquely tracing the Galaxy's molecular clouds, dense, cold strongly-shielded regions where the hydrogen is predominantly molecular and the dominant form of gas phase carbon is CO. Moreover, CO emission plays an especially important role in ISM studies as the tracer of cold molecular hydrogen through the use of the so-called CO-H_2 conversion factor which directly scales the integrated ^{12}CO $J = 1$–0 brightness W_{CO} to H_2 column density N_{H_2}. This deceptively simple conversion is critically important to determining molecular and total gas column densities and so to understanding the most basic properties of star formation (Leroy et al. 2008; Bigiel et al. 2008; Bothwell et al. 2009), the origins of galactic dust emission (Draine et al. 2007), and other such fundamentals.

Yet, it is increasingly recognized that CO emission is present along lines of sight lacking high extinction or large molecular column densities (Liszt & Lucas 1998). It is also the case that some very opaque lines of sight showing CO emission are comprised entirely of diffuse material and H_2-bearing diffuse clouds (McCall et al. 2002): a discussion of such a line of sight from our own work is described in Appendix A here. Even in canonical dark clouds like Taurus, detailed high-resolution mapping of the CO emission (Goldsmith et al. 2008) reveals that much of it originates in relatively weakly-shielded gas where ^{13}CO is strongly enhanced through isotopic fractionation, implying that the dominant form of gas phase carbon must be C^+ (Watson et al. 1976).

Conversely, it is also the case that molecular gas is detected in the local ISM even when CO emission is not. Lines of sight with $N_{CO} \gtrsim 10^{12}$ cm^{-2}, $N_{H_2} \gtrsim 10^{19}$ cm^{-2} have long been detectable in surveys of uv absorption (Sonnentrucker et al. 2007; Burgh et al. 2007; Sheffer et al. 2007, 2008), with expected integrated CO brightnesses as low as $W_{CO} = 0.001$ K km s^{-1} (Liszt 2007b). And, as discussed here, mm-wave HCO^+ and CO absorption from clouds with $N_{H_2} \gtrsim 10^{20}$ cm^{-2} are also more common than CO emission along the same lines of sight (see Lucas & Liszt 1996; Liszt & Lucas 2000, and Appendix A).

Thus we are led to ask two questions that are of particular importance to the use of CO emission as a molecular gas tracer. First, where and how does the observed local CO luminosity really originate? Second, how completely is the molecular material represented by CO emission? The approach we take to address these issues is based on radiofrequency surveys of HI, HCO^+ and CO absorption and emission along lines of sight through the Galaxy toward extragalactic background sources. By combining 1) measurements of extinction (constraining the total gas column density); 2) measurements of HI absorption (to determine the gas column of atomic hydrogen); 3) the strength of HCO^+ absorption (tracing H_2 directly) and 4) the integrated CO $J = 1$–0 brightness W_{CO}, we relate W_{CO} to N_{H_2} along sightlines where we

⋆ Appendix E is only available in electronic form at http://www.aanda.org

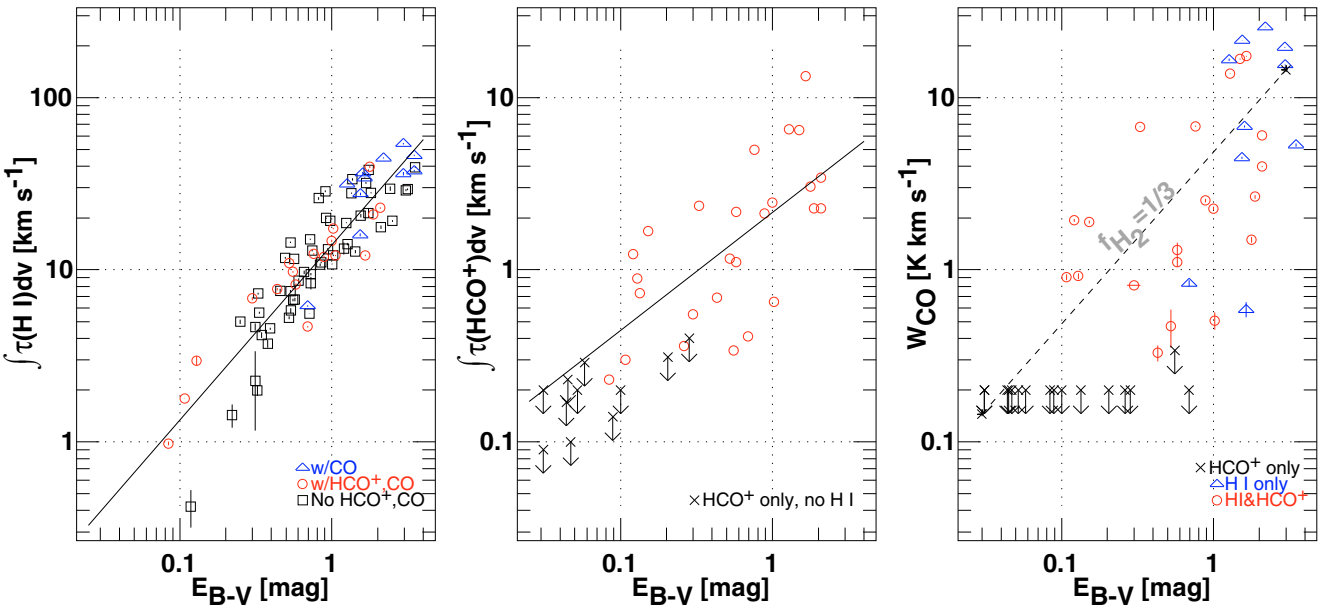

Fig. 1. Atomic and molecular absorption and emission vs. total reddening. *Left*: Integrated VLA HI optical depth from Dickey et al. (1983) and this work. *Middle*: integrated PdBI HCO^+ optical depth from Lucas & Liszt (1996) and this work. *Right*: integrated ARO12m CO J = 1–0 brightness at 1′ resolution. In each case the horizontal axis is the total line of sight reddening E_{B-V} (Schlegel et al. 1998). For explanation of the symbols used in the plots, see Sect. 3.

have previously shown that the intervening gas is diffuse, neither dark nor dense, and the CO column densities are relatively small. The results are somewhat surprising: although there is much variability, the mean CO brightness per H_2-molecule W_{CO}/N_{H_2}, i.e. the CO-H_2 conversion factor, does not differ between diffuse and fully molecular clouds. Although this was phenomenologically inferred long ago, the physical basis for it is now better understood in terms of the radiative transfer and chemistry of H_2- and CO-bearing diffuse and dark gas.

The plan of the present work is as follows. Section 2 describes the observational material that is used here, some of which is new. Section 3 derives the CO-H_2 conversion factor in diffuse gas. Section 4 discusses the fraction of the local galactic CO luminosity (viewed perpendicular to the galactic plane) that can be attributed to diffuse gas. Section 5 discusses the physical processes at play to set the ratio of CO brightness to H_2 column density and explains why the same value may apply to dark and diffuse gas. Section 6 discusses which molecular emission diagnostics might actually be used to distinguish between the CO contributions from diffuse and dark gas. Sections 7 and 8 present a brief summary and discuss how our concept of the ISM might change when a substantial portion of the observed CO emission is ascribed to diffuse rather than dense molecular gas.

2. Observational material

The data used in this work are given in Tables E.1 and E.2 of Appendix E (available online).

2.1. E_{B-V}

Values of the total reddening E_{B-V} along the line of sight are from the work of Schlegel et al. (1998) at a spatial resolution of 6′. The claimed rms error of these measurements is a percentage (16%) of the value. To convert to column density we use the equivalence $N_H = N(H\,I) + 2N_{H_2} = 5.8 \times 10^{21} H\ cm^{-2} E_{B-V}$ established by Bohlin et al. (1978) and Rachford et al. (2009). Typically $A_V = E_{B-V}/3.1$ (Spitzer 1978).

2.2. HI *absorption*

This is mostly taken from the VLA results of Dickey et al. (1983) but a line profile for B2251+158 (3C 454.3) was made available on the website of John Dickey and we took new HI absorption profiles toward J0008+686, J0102+584,B0528+134, B0736+017, J2007+404, J2023+318 and B2145+067 at the VLA in 2005 May and July.

2.3. HCO^+ *absorption*

We used results from the PdBI's HCO^+ survey of Lucas & Liszt (1996) along with the slightly more recent results of Liszt & Lucas (2000) and a few additional profiles that were taken at the PdBI in 2001–2004.

The rotational excitation of HCO^+ above the cosmic microwave background is very weak in diffuse gas (Liszt & Lucas 1996) so that $N_{HCO^+} = 1.12 \times 10^{12}\ cm^{-2} \left(\int \tau(HCO^+)\, dv/1\ km\,s^{-1}\right)$ for an assumed HCO^+ permanent dipole moment of 3.889 Debye. This dipole moment is slightly smaller than the value used in most of our previous work (4.07 D), increasing the inferred HCO^+ column densities by 10%.

2.4. $J = 1–0$ CO *emission*

All the results quoted here are from the ARO12m antenna at 1′ resolution, placed on a main-beam scale by dividing the native T_r^* values by 0.85. Most of these profiles were used on the T_r^* scale in our earlier work (Liszt & Lucas 1996, 1998, 2000) but profiles toward sources with HI absorption and lacking HCO^+ absorption data (noted in Fig. 1) and toward sources with J-names in Tables C.1 and C.2 are new. The velocity resolution was typically 0.1 km s^{-1} and all spectra were taken in frequency-switching mode and deconvolved (folded) using the EKHL algorithm (Liszt 1997a). Where upper limits on CO emission are shown, they are plotted symbolically at very conservative values taken over much wider ranges than are occupied by

HCO^+ emission. The contributions of such sightline to ensemble averages of W_{CO} was taken as zero in each case.

3. The mean N_{H_2}/W_{CO} ratio of diffuse gas

3.1. Considering whole lines of sight

Because the target background sources are extragalactic, the lines of sight considered here traverse the entire galactic gas layer, crossing the entire possible gamut of gas phases. However, they either have low extinction (at $|b| \gtrsim 15$–$20°$) or, more often, can be decomposed into components whose individual molecular column densities are relatively small according to our previous studies of absorption and emission in these directions (see Appendix A for an example). For instance, the highest CO column densities observed for individual components are $N_{CO} \lesssim 2 \times 10^{16}$ cm^{-2} (Liszt & Lucas 1998), representing about 7% of the free carbon column density expected for diffuse ISM at $A_V = 1$ mag (Sofia et al. 2004). ^{13}CO is increasingly strongly fractionated in diffuse clouds having higher N_{CO} (Liszt & Lucas 1998; Liszt 2007a), requiring that carbon must be predominantly in the form of C^+.

3.2. Separating the atomic and molecular gas fractions

In order to derive the N_{H_2}/W_{CO} conversion factor, we need to estimate N_{H_2} independent of the CO emission tracer. To do this, we could use previous estimates of the mean fraction of H_2 in the diffuse ISM, which range from ≳25% (Savage et al. 1977) in uv absorption to 40–45% using a chemically-based approach founded on the observed constancy of $X_{CH} = N_{CH}/N_{H_2}$ (Liszt & Lucas 2002; Sheffer et al. 2008; Weselak et al. 2010). However, as this is the core of our argument, we take two other and more detailed approaches to separating the atomic and molecular column densities along the actual ensemble of lines of sight we have studied. Both methods depend on knowing the total column density N_H from the measured reddening and both are detailed in the following subsections.

3.3. Estimating the atomic gas fraction via HI absorption

In Fig. 1 at left we show the integrated HI absorption plotted against reddening. This diagram is comprised of the entire sample of Dickey et al. (1983) along with a handful of other sightlines observed in HI by us at the VLA and in HCO^+ at the PdBI (see Sect. 2). Symbols differentiate 1) those portions of the sample for which HCO^+ and CO were observed (all sightlines observed in HCO^+ were also observed in CO emission and most in CO absorption); 2) a few for which we only have HI absorption and CO emission data; and 3) those which lack any molecular data. Strictly speaking, only those lines of sight for which we have molecular absorption line data can be proven to be composed wholly of diffuse gas but the sample appears to be very homogeneous in terms of its absorbing properties and many of the lines of sight lacking molecular absorption data show CO emission well beyond the galactic extent of the dense gas layer.

The surprisingly tight, nearly linear correlation between the integrated HI optical depth and reddening (correlation coefficient 0.90, power-law slope 1.02) establishes the applicability of the comparison of reddening values (which are measured on a rather coarse 6′ spatial scale) with HI absorption measurements against the extragalactic continuum sources, sampling sub-arcsecond beams. This excellent correlation between fan and pencil-beam quantities testifies to the high degree to which HI absorbing gas is mixed in the interstellar gas. The sample mean reddening in Fig. 1 at left is $\langle E_{B-V} \rangle = 1.14$ mag and the sample mean integrated HI opacity is $\left\langle \int \tau(\mathrm{HI})\, dv \right\rangle = 16.50\,\mathrm{km\,s^{-1}}$ so that $\left\langle \int \tau(\mathrm{HI})\, dv \right\rangle / \langle E_{B-V} \rangle = 1.45$ km s^{-1}/mag for the sample as a whole.

Estimating the HI column density from the HI absorption must be done with care because the atomic gas is divided between warm and cold phases having widely differing optical depth. Separation of the warm and cold, absorbing and non-absorbing phases was recently considered in great detail by Heiles & Troland (2003) in a new HI emission-absorption survey along many lines of sight. From their tabulated results, it was possible to form the ratio of N_{HI} to $\int \tau(\mathrm{HI})\, dv$ (a small portion of which actually arises in warmer gas) as shown in Fig. B.1 of the appendices and briefly discussed in Sect. B1 there. The sample mean ratio over all lines of sight in the Heiles & Troland (2003) survey is $N_{HI} / \int \tau(\mathrm{HI})\, dv = 2.6 \pm 0.2 \times 10^{20}$ cm^{-2}/km s^{-1} where the error estimate (which is a range, not a standard deviation) reflects the extent to which the ratio can be affected by sample selection criteria based on reddening, galactic latitude, etc. This mean value shows very little variation when computed on subsamples selected on different criteria.

It is then possible to derive the atomic gas fraction, if we assume that our absorption sample has similar properties. Writing

$$f_{HI} \approx \left(\frac{N_{HI}}{\int \tau(\mathrm{HI})\, dv}\right) \times \left(\frac{\int \tau(\mathrm{HI})\, dv}{5.8 \times 10^{21}\, E_{B-V}}\right), \quad (1)$$

taking the first term from our analysis of the results of Heiles & Troland (2003) and the second from the mean for the data shown in Fig. 1. The result is that $f_{HI} = 0.65$, so that $f_{H_2} = 2\, N(H_2)/N(H) = 0.35$.

This estimate of the molecular gas fraction for our sample of sightlines falls in the middle of the range of current general estimates for diffuse gas as noted in the beginning of this Section, i.e. $f_{H_2} \gtrsim 0.25$ from *Copernicus* corrected for sampling biases (Bohlin et al. 1978) and $f_{H_2} \approx 0.40$–0.45 from a sample of lines of sight observed toward bright stars in optical absorption lines observed in CH (Liszt & Lucas 2002), given that $X_{CH} = N_{CH}/N_{H_2}$ is nearly constant at 4.5×10^{-8} (Sheffer et al. 2008; Weselak et al. 2010).

3.4. Checking the molecular gas fraction via molecular chemistry

Shown in the middle panel is the integrated HCO^+ absorption. As noted in Sect. 2.3 the integrated optical depth is directly translatable into HCO^+ column density given the near-absence of rotational excitation in the relatively low density diffuse gas: $N_{HCO^+} = 1.12 \times 10^{12}$ cm^{-2} $\left(\int \tau(\mathrm{HCO^+})\, dv / 1\,\mathrm{km\,s^{-1}}\right)$. The relative abundance of HCO^+ is known to be nearly constant at $X_{HCO^+} \simeq 2$–3×10^{-9} from its fixed ratio with respect to OH in individual clouds (Liszt & Lucas 1996, 2000) and the near-constancy of $X_{OH} \approx 10^{-7}$ (Weselak et al. 2010).

Figure 1 shows that HCO^+ becomes readily detectable at $E_{B-V} \gtrsim 0.1$ mag, which is just where H_2 itself becomes abundant in the diffuse ISM (Savage et al. 1977). When detected, N_{HCO^+} shows a correlation with E_{B-V} (correlation coefficient 0.66 and power law slope 0.7 for the points with detected HCO^+) but the larger scatter in the middle panel, compared to that at left, suggests that the molecular portion of the gas is less well mixed than the absorbing HI.

If X_{HCO^+} is assumed, a value for f_{H_2} could be derived from the data in the middle panel of Fig. 1. Conversely, if $f_{H_2} = 0.35$ is assumed and sample means are used, then $\langle N_{HCO^+}\rangle / (5.8 \times 10^{21}\ \mathrm{cm^{-2}}\ \langle E_{B-V}\rangle) = 5.46 \times 10^{-10}$ and $X_{HCO^+} = N_{HCO^+}/N_{H_2} = 3.1 \times 10^{-9}$, consistent with the previously established value (Liszt & Lucas 1996, 2000). Therefore the decomposition of the ensemble of lines of sight appears to yield consistent results between several independent measures of both the atomic and molecular components.

3.5. The ensemble-averaged CO luminosity and N_{H_2}/W_{CO} conversion factor

Shown at the right in Fig. 1 is the integrated ^{12}CO $J = 1$–0 intensity W_{CO} plotted against E_{B-V}. CO emission is not reliably detected except at $E_{B-V} > 0.3$ mag (i.e. $A_V \gtrsim 1$ mag). In discussing this data, it is important to note that values of N_{CO} have been measured in the diffuse gas (Liszt & Lucas 1998) and they are quite small compared to the column of free gas phase carbon expected at $A_V = 1$ mag (i.e. 3×10^{17} cm^{-2}, see Sofia et al. 2004). Moreover, the lines of sight having the largest values of W_{CO} are composed of several emission components (see Appendix A for an example). The CO emission along these lines of sight orginates in diffuse gas where C^+ is the dominant form of carbon.

If it is accepted that $f_{H_2} = 0.35$, the bulk CO-H_2 conversion factor may be inferred immediately from the data shown in Fig. 1. The sample means are $\langle W_{CO}\rangle = 4.42$ K km s^{-1} and $\langle E_{B-V}\rangle = 0.888$ mag or ($\langle N_{H_2}\rangle = 9.01 \times 10^{20} H_2$ cm^{-2}), implying $W_{CO} = 1$ K km s^{-1} per 2.04×10^{20} H_2 cm^{-2}. Rather strikingly, there is apparently no difference in the *mean* CO luminosity per H_2 in diffuse and fully molecular gas. For insight into the scatter present in the ensemble of sightlines, the right-hand panel of Fig. 1 shows a line corresponding to the ensemble mean conversion factor and $f_{H_2} = 1/3$. The range in f_{H_2} determined for the diffuse gas, roughly 0.25–0.45 or 0.35 ± 0.1, implies a 30% margin of error for the method as a whole.

An alternative approach to this determination based on molecular chemistry, comparing W_{CO} with N_{HCO^+} as a surrogate for N_{H_2} and giving similar results, is discussed in Appendix C.

4. The proportion of CO emission arising from diffuse gas

The similarity of the CO-H_2 conversion factors in diffuse and fully molecular gas must have led to confusion whereby CO emission arising in diffuse gas has been attributed to "molecular clouds", i.e. the truism noted in the Introduction. To quantify this phenomenon we derive the mean luminosity of diffuse molecular gas viewed perpendicular to the galactic plane $W_{CO}(b) \sin|b|$ for a plane-parallel stratified gas layer and we compare that to the equivalent luminosity perpendicular to the galactic plane inferred from surveys of CO emission near the galactic equator.

Shown in Fig. 2 is the distribution of W_{CO} with $1/\sin|b|$. For reference a line is shown corresponding to the canonical CO-H_2 conversion factor and the combination $f_{H_2} \times \sigma_z = 30$ pc, in the simplistic case that the galactic gas layer can be described by a single Gaussian vertical component with dispersion σ_z. For convenience the diffuse gas is usually described by several components having a range of vertical scale heights (Cox 2005) but the neutral gas components of the nearby ISM are not well-described by simple plane-parallel layers (see also Heiles & Troland 2003) owing to local geometry (the local bubble)

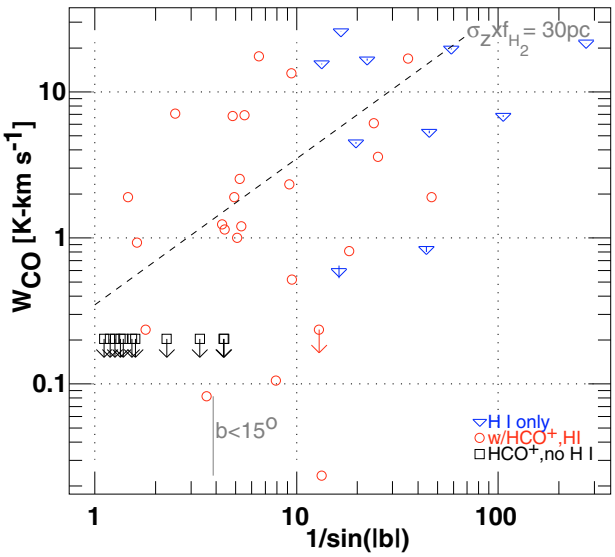

Fig. 2. Integrated CO brightness plotted against $1/\sin(|b|)$. For comparison, a line is shown for the case of a plane-parallel Gaussian layer with vertical dispersion σ_z, when $\sigma_z f_{H_2} = 30$ pc and $N_{H_2}/W_{CO} = 2 \times 10^{20}$ H_2 cm^{-2}/(K km s^{-1}).

combined with the scatter induced by the comparatively long mean free paths between kinematic components.

We quote the ensemble average brightness $\langle W_{CO}\rangle = 4.64$ K km s^{-1} and number of equivalent half-thicknesses $\langle 1/\sin|b|\rangle = 19.75$, implying a mean integrated brightness 0.235 K km s^{-1} per galactic half width[1]. Looking down on the Milky Way vertically from afar the integrated CO brightness of diffuse gas would be twice this, $W_{CO_\perp} = 0.47$ K km s^{-1}.

Galactic surveys of CO emission, on the other hand, calculate a mean CO brightness per kpc of 5 K km s^{-1}/kpc at $z = 0$ pc in the galactic disk at a galactocentric distance $R_\odot = 8$ kpc. Note that this value is scaled from the result of Burton & Gordon (1978) which assumed $R_\odot = 10$ kpc. If the molecular gas layer sampled in these surveys is described by a Gaussian vertical distribution having a dispersion $\sigma_z = 60$ pc (Cox 2005) and z-integral $\sqrt{2\pi\sigma_z^2} = 0.150$ kpc, the galactic survey result translates into an integrated CO brightness $W_{CO_\perp} = 5$ K km s^{-1}/kpc $\times$ 0.150 kpc = 0.75 K km s^{-1} when viewed vertically across the galactic disk as described in Appendix D. This is only 50% higher than that of the diffuse CO alone.

The question then is whether the CO emission and H_2 attributable to diffuse gas exist in addition to that sampled in the CO surveys near the galactic plane, or whether the galactic CO surveys incorporate a significant proportion of diffuse CO emission. If the former – if, for instance the diffuse CO like the diffuse ISM has a larger scale height and is a distinguishable component of the local CO emission – the local H_2 surface density could be higher than previously believed.

The total density of gas near the Sun is usually quoted as 1.2 H-nuclei cm^{-3} from Spitzer (1978) and this is often decomposed into "molecular" and "diffuse" components with roughly 50% attributed to each (for instance see Cox 2005). The CO emissivity measured in galactic plane surveys (5 K km s^{-1}/kpc) conveniently converts to a local mean H_2 density of about 0.33 H_2 cm^{-3}, about half of Spitzer's total. However, recall that the quoted total mean density is based on the statistics of reddening toward A-stars within a few hundred pc of the Sun

[1] The actual ensemble averaged value of $\langle W_{CO} \sin|b|\rangle$ is substantially larger 0.42 ± 0.66 K km s^{-1}.

(Münch 1952) which were very unlikely to have sampled dark cloud lines of sight. GAIA photometry should settle this matter, but the issue of the total mean density of the ISM locally and relative proportions of atomic and molecular material are not as clearly defined as is generally assumed.

5. Rationale for a common CO-H_2 conversion

The very first discussions of the applicability of a common N_{H_2}/W_{CO} conversion factor (Liszt 1982; Young & Scoville 1982) noted that diffuse and dense gas at 60–100 K, or dark dense gas at 12 K, all had similar ratios W_{CO}/N_{H_2}. For instance $W_{CO} \approx 1.5$ K km s^{-1}, $N_{H_2} = 5 \times 10^{20}$ km s^{-1} toward ζ Oph (a typical diffuse line of sight) and $W_{CO} = 450$ K km s^{-1}, $N_{H_2} = 2 \times 10^{23}H_2$ cm^{-2} toward Ori A. By comparison, a dark cloud like L204, near ζ Oph, with $A_V = 5$ mag has $N_{H_2} \approx 5 \times 10^{21}$ cm^{-2}, $N_{CO} \approx 8 \times 10^{17}$ cm^{-2} and an integrated brightness $W_{CO} \approx 15$ K km s^{-1} (Tachihara et al. 2000) or $N_{H_2}/W_{CO} \approx 3 \times 10^{20}H_2$ cm^{-2} (K km s)$^{-1}$. Comparing the two gas phases sampled in CO near ζ Oph it is apparent that the higher CO column density in the dark cloud is more than compensated by the diminished brightness per CO molecule. The result is a nearly constant ratio of W_{CO} to N_{H_2} across phases while the brightness per CO molecule W_{CO}/N_{CO} varies widely.

The physical basis for this behavior has become more apparent recently with closer study of CO in diffuse gas (Pety et al. 2008; Liszt et al. 2009). To begin the discussion we rewrite the CO-H_2 conversion factor χ_{CO} as

$$\frac{1}{\chi_{CO}} = \left(\frac{W_{CO}}{N_{CO}}\right) \times \left(\frac{N_{CO}}{N_{H_2}}\right) = \left(\frac{W_{CO}}{N_{CO}}\right) X_{CO}, \quad (2)$$

separating the coupled and competing effects of cloud structure or radiative transfer (W_{CO}/N_{CO}) and CO chemistry ($N_{CO}/N_{H_2} = X_{CO}$). Simply put, the specific brightness W_{CO}/N_{CO} can be shown to be higher in warmer, subthermally-excited diffuse gas by about the same amount (a factor 30–50) that X_{CO} is lower: $\langle X_{CO} \rangle = 3 \times 10^{-6}$ for the diffuse gas (Burgh et al. 2007) compared to $\approx 10^{-4}$ in dark gas where the carbon is very nearly all in CO.

As noted by Goldreich & Kwan (1974) in the original exposition of the LVG model for radiative transfer, W_{CO}/N_{CO} will be much greater when the excitation of CO is weak – when the kinetic temperature is much greater than the $J = 1$–0 excitation temperature. Moreover when CO is excited somewhat above the cosmic microwave background but well below the kinetic temperature, the brightness of the CO $J = 1$–0 line will be linearly proportional to N_{CO} even when the line is quite optically thick (again, see Goldreich & Kwan 1974). As Michel Guelin pointedly reminded us, this occurs because weak excitation means that there is also little collisional de-excitation so that the gas merely scatters emitted photons until they eventually escape. As Goldreich & Kwan (1974) showed, this proportionality between brightness and column density persists until the opacity is so very large that the transition approaches thermalization through radiative trapping.

The discussion of the previous paragraph also applies to other molecules, but because CO has such a small dipole moment the proportionality between CO brightness and column density is only weakly dependent on ambient physical conditions: a nearly universal ratio $N_{CO}/W_{CO} = 10^{15}$ CO cm^{-2}/(K km s^{-1}) can be calculated for diffuse gas using recent excitation cross-sections (Liszt 2007b). This is in excellent agreement with measured values of N_{CO} and CO $J = 1$–0 excitation temperatures in the diffuse gas seen toward stars in uv absorption (Sonnentrucker et al. 2007; Burgh et al. 2007; Sheffer et al. 2008) or at mm-wavelengths in absorption against distant quasars (Liszt & Lucas 1998). For the observed value $\langle X_{CO} \rangle = 3 \times 10^{-6}$ (Burgh et al. 2007) the N_{H_2}/W_{CO} conversion ratio in diffuse clouds is $N_{H_2}/W_{CO} = 10^{15}/3 \times 10^{-6} = 3.3 \times 10^{20}$ H$_2$ cm^{-2}/(K km s^{-1}).

Finally, note that even if the ratio W_{CO}/N_{CO} is not constant between gas phases, it is still the case that $W_{CO} \propto N_{CO}$ separately in either the dense or diffuse gas. For the diffuse gas the proportionality is based in the microphysics of CO radiative transfer a la Goldreich & Kwan (1974). For the dark cloud case, note that there is a fixed ratio of N_{CO}/N_{H_2} when the gas-phase carbon is in CO and the hydrogen is in H_2 so that a W_{CO}–N_{H_2} conversion is fully equivalent to a W_{CO}–N_{CO} conversion.

6. Discriminating between emission from diffuse and dense gas

There are ways in which mm-wave molecular emission differs between dense and diffuse gas, even if not in ^{12}CO. Emission from molecules like CS, HCN and HCO$^+$ having higher dipole moments is generally thought to single out denser gas than does CO, especially in extreme environments (Wu et al. 2005). Note, however, that surveys of the Milky Way galactic plane find widely-distributed emission in HCO$^+$, CS, HCN, etc. with intensity ratios of 1–2% relative to W_{CO} from essentially all features detected in CO (Liszt 1995; Helfer & Blitz 1997).

Relatively little is known of the emission from mm-wave species in diffuse gas beyond that from CO. Most common is emission from HCO$^+$ because it is chemically ubiquitous and somewhat more easily excited owing to its positive charge and high dipole moment. Although HCO$^+$ emission is weak in the example shown here in Appendix A it appears at levels $\gtrsim$1% of W_{CO} in portions of the diffuse cloud around ζ Oph or in the Polaris flare (Liszt & Lucas 1994; Liszt 1997; Falgarone et al. 2006). Therefore HCO$^+$ emission is probably not a good discriminator but CS and HCN appear with high abundance only when $N_{HCO^+} \gtrsim 10^{12}$ cm^{-2} or $N_{H_2} > 5 \times 10^{20}$ cm^{-2} and should be much more weakly excited in low density gas. In any case, searching for emission that is 100 times weaker than W_{CO} may not be an effective use of observing time and only in very dense, warmer gas like that found in massive, OB star-forming regions like Ori A are the higher dipole moment molecules substantially brighter than 1–2% relative to W_{CO}.

A more effective method of discriminating between CO emission from diffuse and dark or dense gas is afforded by ^{13}CO. Although the abundance of ^{13}CO is enhanced by fractionation (see the example in Appendix A) lowering the observed ^{12}CO/^{13}CO brightness temperature ratios (Liszt & Lucas 1998; Liszt 2007b; Goldsmith et al. 2008), those ratios are still noticeably higher in diffuse gas. Typically they are $\gtrsim$10–15 instead of $\lesssim$3–5 as seen in dark clouds or in surveys of the inner-Galaxy gas in the galactic plane (Burton & Gordon 1978). Recall that the mean ^{12}CO/^{13}CO brightness ratio nearly doubles across the galactic disk (Liszt et al. 1981), which was another, earlier indication that molecular gas near the Solar Circle has a high proportion of diffuse material.

To summarize, we suggest that the most efficient way to ascertain the origin of CO emission is to compare ^{12}CO and ^{13}CO brightnesses because emission from ^{13}CO is much stronger than emission from HCO$^+$, CS, HCN etc., and because there is actually less ambiguity in the brightness ratios relative to W_{CO}.

7. Summary

In Sects. 2 and 3 we described and considered a sample of lines of sight studied in HI and molecular absorption and known to be comprised of diffuse gas. Their molecular component shows features whose CO, HCO^+ and other molecular column densities are small compared to those of dark clouds (in the case of CO, at least 30 times smaller). There is often quite substantial fractionation of ^{13}CO (indicating that the dominant form of carbon is C^+) and the rotational excitation of CO is sub-thermal with implied cloud temperatures typical of those determined directly for diffuse H_2 in optical/uv surveys, i.e. 30 K or more.

Using an externally-determined value for the ratio of total HI column density to integrated HI absorption and the standard equivalence between reddening and N_H we derived the molecular gas fraction for this sample to be $f_{H_2} = 0.35$, in the middle of the range of other estimates for the diffuse ISM as a whole based on optical (mainly CH) and uv (HI and H_2) absorption studies.

We showed that this estimate for f_{H_2} implies the same value $X_{HCO^+} = 3 \times 10^{-9}$ that was previously determined from comparisons of OH and HCO^+ column densities in individual clouds. We then compared measured CO brightnesses with the inferred molecular gas column densities to derive the ensemble mean N_{H_2}/W_{CO} conversion factor. Surprisingly, We found this mean to be just equal to the locally-accepted value $2.0 \times 10^{20} H_2/(\mathrm{K\,km\,s^{-1}})$ for "molecular" gas believed to reside in dense dark fully-molecular clouds near the galactic equator.

Such exact agreement is probably something of an accident of sampling, but the fact that diffuse and dark gas would have very similar N_{H_2}/W_{CO} conversion factors, which had been inferred empirically long ago, now has a firmer physical basis. In Sect. 5 we explained it as the result of the brightening of CO $J = 1$–0 emission per CO molecule that was theoretically predicted for warmer more diffuse gas by Goldreich & Kwan (1974), which compensates for the lower relative abundance X_{CO} there. The mean CO abundance observed in optical absorption in diffuse clouds $\langle X_{CO} \rangle = 3 \times 10^{-6}$, combined with the observed and expected brightness per CO molecule, $W_{CO}/N_{CO} = 1\ \mathrm{K\,km\,s^{-1}}/10^{15} \mathrm{CO\ cm^{-2}}$, can be be combined to form an CO-H_2 conversion factor of $N_{H_2}/W_{CO} = 10^{15}/3{\times}10^{-6} = 3.3 \times 10^{20}\,\mathrm{H_2\,cm^{-2}/(K\,km\,s^{-1})}$.

In Sect. 4 we derived the expected brightness of diffuse gas viewed perpendicular to the galactic plane from afar, $0.47\,\mathrm{K\,km\,s^{-1}}$, and compared that to the value expected from surveys of CO emission in the galactic plane, combined with a narrow (60 pc dispersion) Gaussian vertical distribution; that is $0.75\,\mathrm{K\,km\,s^{-1}}$. This suggests that there has been confusion in the general attribution of CO emission to "molecular clouds" when in fact much of it arises in the diffuse ISM. This view is consistent with the motivations discussed in the Introduction, whereby CO emission is increasingly being found along lines of sight lacking high extinction and whereby CO emission seen along dark lines of sight is found (through molecular absorption studies and in other ways) to originate in components having the relatively small molecular number and column densities typical of diffuse gas. An example of such a line of sight is given in Appendix A here.

We briefly discussed in Sect. 4 the decomposition of the total mean density of neutral gas in the nearby ISM, 1.2 H $\mathrm{cm^{-3}}$ (Spitzer 1978), into its atomic and molecular constituents. We noted that although the balance is generally believed to be roughly 50–50 (Cox 2005), some emission might shift to the diffuse side of the balance sheet if CO emission is reinterpreted. Moreover, we pointed out that the molecular contribution to the true local mean density from large-scale galactic CO surveys in the galactic plane should be questioned more generally because it is unclear to what extent Spitzer's estimate, based on the earlier optical work of Münch, incorporates the contribution of optically-opaque gas.

Although the ability to discriminate between the separate contributions to W_{CO} from diffuse and darker, denser gas is limited when only ^{12}CO is considered, it should be possible to infer the nature of the host gas using other emission diagnostics (see Sect. 6). The most efficient of these is probably the brightness of ^{13}CO, which, although enhanced by fractionation, is still substantially weaker, relative to W_{CO}, in diffuse gas. Searching for emission from species having higher dipole moments such as CS $J = 2$–1 and HCN (and probably not HCO^+ because it is chemically so ubiquitous and more easily excited) are alternatives that might require somewhat longer integration times.

8. Discussion: Interpreting a sky occupied by CO emission from diffuse gas

The usual interpretation of CO sky maps, galactic surveys, etc, is that CO emission mostly traces dark and or "giant" molecular clouds (GMC) composed of dense cold gas occupying a very small fraction of the interstellar volume at high thermal pressure within an ISM that may confine them via its ram or turbulent pressure if they are not gravitationally bound. The balance between GMC and diffuse atomic material may be controlled by quasi-equilibrium between local dynamics and the overlying weight of the gas layer but the molecular material inferred from CO emission is generally believed to be that which is most nearly on the verge of forming stars, for instance through the Schmidt-Kenicutt power-law relation between star formation rate and gas surface density[2] (Leroy et al. 2008; Bigiel et al. 2008).

By contrast, CO emission from diffuse molecular gas originates within a warmer, lower-pressure medium that occupies a much larger fraction of the volume and contributes more substantially to mid-IR dust or PAH emission but only has the requisite density and chemistry to produce CO molecules and CO emission (since $W_{CO} \propto N_{CO}$) over a very limited portion of that volume. In this case a map of CO emission is a map of CO abundance and CO chemistry first, and only secondarily a map of the mass even if the mean CO-H_2 conversion ratio is (as we have shown) "standard". Moreover, although CO emission traces the molecular column density N_{H_2} quite decently where W_{CO} is at detectable levels, it arises in regions that are not gravitationally bound or about to form stars. The CO sky is mostly an image of the CO chemistry.

Acknowledgements. The National Radio Astronomy Observatory is operated by Associated Universites, Inc. under a cooperative agreement with the US National Science Foundation. The Kitt Peak 12-m millimetre wave telescope is operated by the Arizona Radio Observatory (ARO), Steward Observatory, University of Arizona. IRAM is operated by CNRS (France), the MPG (Germany) and the IGN (Spain). This work has been partially funded by the grant ANR-09-BLAN-0231-01 from the French *Agence Nationale de la Recherche* as part of the SCHISM project. We thank Bob Garwood for providing the H I profiles of Dickey et al. (1983) in digital form.

Appendix A: NRAO150: an example of a dark line of sight comprised of diffuse gas

The estimated total extinction along this comparatively low-latitude line of sight at $l = 150.4°$, $b = -1.6°$ (see Table E.2)

[2] It is also recognized that more precise tracers of the high-density star-forming material may be needed in extreme environments such as ULIRG (Wu et al. 2005).

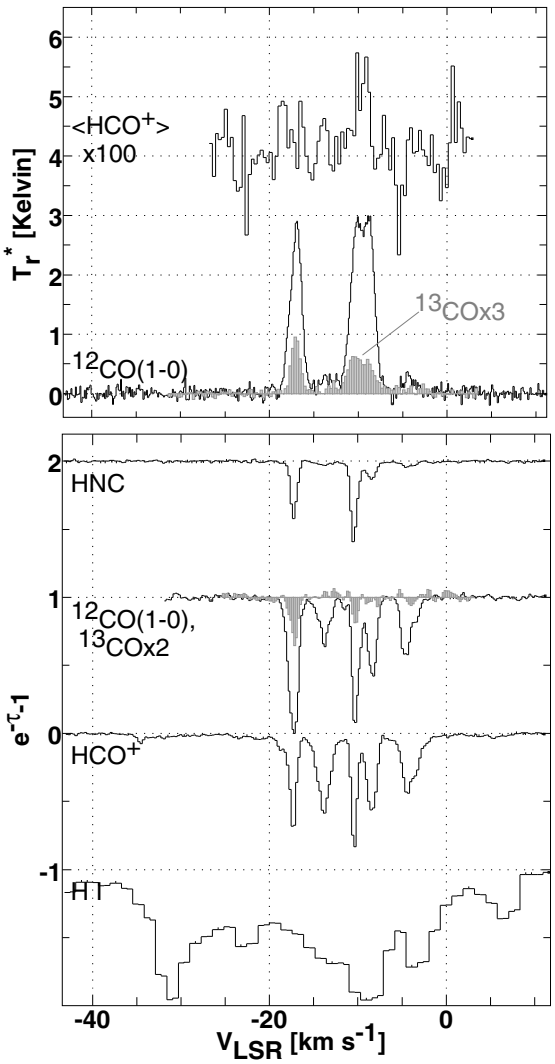

Fig. A.1. Line profiles toward and near B0355+508 = NRAO150. *Bottom*: absorption line profiles of H I, HCO^+, ^{12}CO, ^{13}CO (multiplied by 2) and HNC; HI absorption and emission are present over a much broader velocity range than shown here. *Top*: Emission from ^{12}CO, ^{13}CO (scaled upward by a factor 3) and HCO^+ (scaled upward by a factor 100). The HCO^+ profile is an average over a 3.5′ region around the continuum (to avoid absorption). See Appendix A.

is E_{B-V} = 1.5 mag or $A_V \approx$ 5 mag but it would be quite opaque even if only the atomic gas were present. A lower limit on N_{HI} from the integrated 21 cm emission of the nearest profile in the Leiden-Dwingeloo Survey (Hartmann & Burton 1997) in the optically thin limit is $N_{HI} \gtrsim 7.4 \times 10^{21}$ cm^{-2}, implying $E_{B-V} \gtrsim 1.27$ mag. The H I column density derived by taking the ratio of N_{HI} to HI absorption as discussed in Sect. 3 here is, understandably, slightly larger, $N_{HI} = 1.1 \times 10^{22}$ cm^{-2}.

We show in Fig. A.1 various absorption and emission profiles along and around the line of sight to NRAO150 aka B0355+508. We have published various analyses of this line of sight in the references noted below, and most recently we synthesized the CO emission in a 90″ region around NRAO150 at 6″ resolution (Pety et al. 2008). HI absorption and emission extend well outside the narrow kinematic interval shown here. The weak HCO^+ absorption at −35 km s^{-1} is real, as is the broad wing extending up to −25 km s^{-1}.

CO emission is fairly strong in this direction, W_{CO} = 17 K km s^{-1}, nominally implying $2N_{H_2} \approx 7 \times 10^{21}$, comparable to N_{HI}, but molecular absorption spectra of HCO^+ and CO

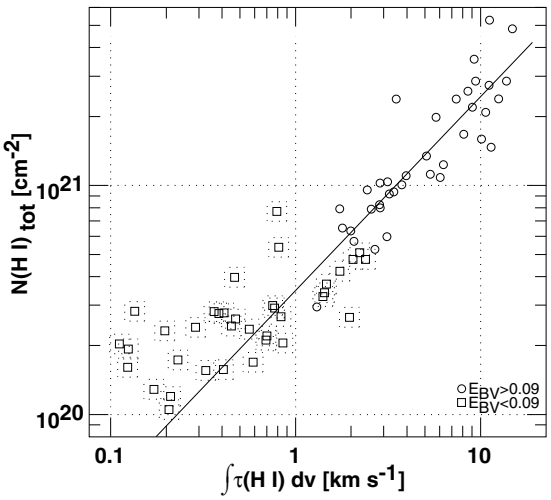

Fig. B.1. Total hydrogen column density vs. integrated HI optical depth for the sources studied by Heiles & Troland (2003). Lines of sight with $E_{B-V} < 0.09$ mag were not included in the regression fit, to point out the upturn at low $\int \tau(\mathrm{HI})\, dv$. See Appendix B.

are much richer than the CO emission. The HCO^+ absorption spectrum (Lucas & Liszt 1996; Liszt & Lucas 2000) shows five prominent components each having $N_{HCO^+} \approx 1.3 \times 10^{12}$ cm^{-2} (Lucas & Liszt 1996) or $2N_{H_2} \approx 9 \times 10^{20}$ cm^{-2} implying E_{B-V} = 0.15 mag per component associated with H_2 if $X_{HCO^+} = 3 \times 10^{-9}$ as discussed in Sect. 3. The H_2, HCO^+ and OH column densities of these components are each nearly equal to what is seen locally along the line of sight to ζ Oph at A_V = 1 mag (Morton 1975; Van Dishoeck & Black 1986; Liszt 1997).

Further evidence of the diffuse nature of the gas is given by the fractionation of ^{13}CO in CO; $N_{^{12}CO}/N_{^{13}CO} = 15 \pm 2$, 25 ± 4 and 32 ± 13 in the components at −17, −11 and −4 km s^{-1}, respectively and $N_{^{13}CO}/N_{C^{18}O} > 36$, >54 and >25 at the 2σ level in these components (Liszt & Lucas 1998).

In emission, the $^{12}CO/^{13}CO$ brightness ratios are 12 and 30 for the two strong kinematic components, reflecting both the fractionation and the fact that $W_{CO} \propto N_{CO}$ in the diffuse gas regime as discussed in the text here.

HCO^+ emission is weak in Fig. A.1. The profile shown (from Lucas & Liszt 1996) is an average of positions around the continuum source to avoid contamination from absorption. The low levels of HCO^+ emission seen toward our sample of background continuum sources can be understood as arising from relatively low density gas ($n_{H_2} \lesssim 100$ cm^{-3}) when the electron fraction is as high as expected for diffuse gas, i.e. 2×10^{-4} (Lucas & Liszt 1994, 1996).

Appendix B: The ratio of total to absorbing HI

Shown in Fig. B.1 is a plot of the data from the tables of Heiles & Troland (2003) that were used in Sect. 3 to convert the $\int \tau(\mathrm{HI})\, dv$ measurements in Fig. 1 to a total quantity of HI. The plot shows a regression line (power-law slope 0.84) fit to data points with $E_{B-V} > 0.09$ mag (the range occupied by the HCO^+ *detections* in Fig. 1) to point out a slight upturn at low $\int \tau(\mathrm{HI})\, dv$. The sample means are largely unaffected by setting various sample selection criteria.

Appendix C: A chemistry-based determination of N_{H_2}/W_{CO}

It is also possible to determine W_{CO}/N_{H_2} without the H I measure or formally estimating f_{H_2}, although we preferred not to

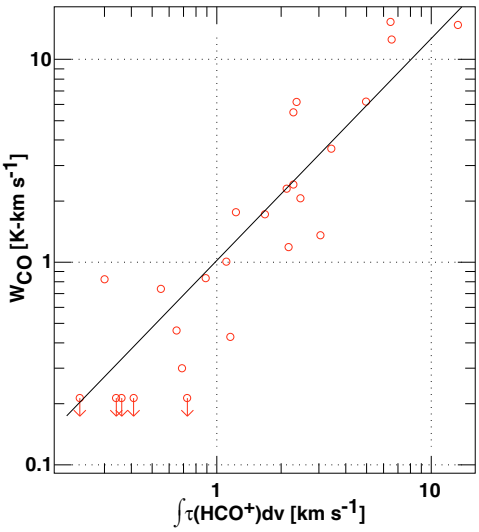

Fig. C.1. Integrated CO $J = 1$–0 brightness plotted against the integrated HCO^+ $J = 1$–0 optical depth. $N_{HCO^+} = 1.12 \times 10^{12}$ cm^{-2} $\left(\int \tau(HCO^+)\,dv/1\ \mathrm{km\,s^{-1}}\right)$. See Appendix D.

do this in the main discussion. In Fig. C.1 we show the variation of W_{CO} with $\int \tau(HCO^+)\,dv$. CO appears reliably at detectable levels $W_{CO} \gtrsim 0.3\,\mathrm{K\,km\,s^{-1}}$, $N_{CO} \gtrsim 3 \times 10^{14}$ cm^{-2} when $N_{HCO^+} \gtrsim 3 \times 10^{11}$ cm^{-2} or $N_{H_2} \gtrsim N_{HCO^+}/3 \times 10^{-9} = 10^{20}$ cm^{-2}. If $X_{HCO^+} = 3 \times 10^{-9}$ the ensemble mean values $\langle W_{CO}\rangle = 3.45\,\mathrm{K\,km\,s^{-1}}$, $\left\langle \int \tau(HCO^+)\,dv \right\rangle = 2.38\,\mathrm{km\,s^{-1}}$ imply $W_{CO} = 1\ \mathrm{K\,km\,s^{-1}}$ per 2.6×10^{20} H_2 cm^{-2}, just 30% above that derived in Sect. 3.5.

The near linearity of the N_{CO}–N_{HCO^+} relationship in Fig. C.1 results from bulk averaging over whole lines of sight: given the same general mix of conditions, an ensemble of richer and poorer or shorter and longer sightlines will show proportionalities between almost any two quantities in this way. As shown in Fig. A.1 there is no such proportionality on a per-component basis. In detail, and with much scatter, the overall chemical variation is approximately $N_{CO} \propto (N_{H_2})^2$ (Liszt 2007b; Sheffer et al. 2008).

Appendix D: Calculating the CO brightness from galactic survey results

The statistics of observing the clumpy galactic molecular cloud distribution are Poisson (Gordon & Burton 1976; Burton & Gordon 1978) so the integrated CO brightness $W_{CO}(r)$ accumulated when traversing a path of length r in the galactic plane is

$$W_{CO}(r) = W_{CO_0}(1 - \exp(-r/\lambda)) \qquad (D.1)$$

where W_{CO_0} is the characteristic brightness of a clump (GMC) and λ is the geometric mean free path between clumps. Although it is possible to derive W_{CO_0} and λ separately, galactic survey results are given in terms of a hybrid quantity A_{CO} whose units are $\mathrm{K\,km\,s^{-1}}$ per kpc corresponding to evaluating $W_{CO}(r)$ when $r \ll \lambda$, i.e. $W_{CO}(r) = (W_{CO_0}/\lambda)\ r = A_{CO}\ r$. The coefficient A_{CO} is closely related to the mean density: just convert W_{CO} to N_{H_2}. For H I the integrated brightness per unit distance is directly converted into a mean density n(H I), if it is assumed that the gas is optically thin.

The brightness of the CO cloud ensemble viewed vertically through the galactic disk is then just $A_{CO}\,\Delta z$, where Δz is the equivalent thickness of the disk. For a Gaussian vertical distribution with dispersion σ_z, $\Delta z = (2\pi)^{1/2}\sigma_z$.

References

Bigiel, F., Leroy, A., Walter, F., et al. 2008, AJ., 136, 2846
Bohlin, R. C., Savage, B. D., & Drake, J. F. 1978, ApJ, 224, 132
Bothwell, M. S., Kennicutt, R. C., & Lee, J. C. 2009, MNRAS, 400, 154
Burgh, E. B., France, K., & McCandliss, S. R. 2007, ApJ, 658, 446
Burton, W. B., & Gordon, M. A. 1978, A&A, 63, 7
Cox, D. P. 2005, ARA&A, 43, 337
Dickey, J. M., Kulkarni, S. R., Heiles, C. E., & Van Gorkom, J. H. 1983, ApJSS, 53, 591
Draine, B. T., Dale, D. A., Bendo, G., et al. 2007, ApJ, 663, 866
Falgarone, E., Pineau Des Forêts, G., Hily-Blant, P., & Schilke, P. 2006, A&A, 452, 511
Garwood, R. W., & Dickey, J. M. 1989, ApJ, 338, 841
Goldreich, P., & Kwan, J. 1974, ApJ, 189, 441
Goldsmith, P. F., Heyer, M., Narayanan, G., et al. 2008, ApJ, 680, 428
Gordon, M. A., & Burton, W. B. 1976, ApJ, 208, 346
Hartmann, D., & Burton, W. B. 1997, Atlas of galactic neutral hydrogen (Cambridge; New York: Cambridge University Press)
Heiles, C., & Troland, T. H. 2003, ApJ, 586, 1067
Helfer, T. T., & Blitz, L. 1997, ApJ, 478, 233
Leroy, A. K., Walter, F., Brinks, E., et al. 2008, AJ, 136, 2782
Liszt, H. 1997a, A&ASS, 124, 183
Liszt, H. S. 1982, ApJ, 262, 198
Liszt, H. S. 1995, ApJ, 442, 163
Liszt, H. S. 1997, A&A, 322, 962
Liszt, H. S. 2007a, A&A, 476, 291
Liszt, H. S. 2007b, A&A, 461, 205
Liszt, H., & Lucas, R. 2002, A&A, 391, 693
Liszt, H. S., & Lucas, R. 1994, ApJ, 431, L131
Liszt, H. S., & Lucas, R. 1996, A&A, 314, 917
Liszt, H. S., & Lucas, R. 1998, A&A, 339, 561
Liszt, H. S., & Lucas, R. 2000, A&A, 355, 333
Liszt, H. S., Burton, W. B., & Bania, T. M. 1981, ApJ, 246, 74
Liszt, H. S., Pety, J., & Tachihara, K. 2009, A&A, 499, 503
Lucas, R., & Liszt, H. S. 1994, A&A, 282, L5
Lucas, R., & Liszt, H. S. 1996, A&A, 307, 237
McCall, B. J., Hinkle, K. H., Geballe, T. R., et al. 2002, ApJ, 567, 391
Morton, D. C. 1975, ApJ, 197, 85
Münch, I. G. 1952, ApJ, 116, 575
Pety, J., Lucas, R., & Liszt, H. S. 2008, A&A, 489, 217
Rachford, B. L., Snow, T. P., Destree, J. D., et al. 2009, ApJSS, 180, 125
Savage, B. D., Drake, J. F., Budich, W., & Bohlin, R. C. 1977, ApJ, 216, 291
Schlegel, D. J., Finkbeiner, D. P., & Davis, M. 1998, ApJ, 500, 525
Sheffer, Y., Rogers, M., Federman, S. R., et al. 2008, ApJ, 687, 1075
Sheffer, Y., Rogers, M., Federman, S. R., Lambert, D. L., & Gredel, R. 2007, ApJ, 667, 1002
Sofia, U. J., Lauroesch, J. T., Meyer, D. M., & Cartledge, S. I. B. 2004, ApJ, 605, 272
Sonnentrucker, P., Welty, D. E., Thorburn, J. A., & York, D. G. 2007, ApJSS, 168, 58
Spitzer, L. 1978, Physical processes in the interstellar medium (New York: Wiley-Interscience)
Tachihara, K., Abe, R., Onishi, T., Mizuno, A., & Fukui, Y. 2000, Publ. Astron. Soc. Jpn., 52, 1147
Van Dishoeck, E. F., & Black, J. H. 1986, ApJSS, 62, 109
Watson, W. D., Anicich, V. G., & Huntress, W. T., J. 1976, ApJ, 205, L165
Weselak, T., Galazutdinov, G. A., Beletsky, Y., & Krełowski, J. 2010, Mon. Not. R. Astron. Soc., 402, 1991
Wu, J., Evans, II, N. J., Gao, Y., et al. 2005, ApJ, 635, L173
Young, J. S., & Scoville, N. 1982, ApJ, 258, 467

Pages 9 to 10 are available in the electronic edition of the journal at http://www.aanda.org

Appendix E: Data

The data shown in Fig. 1 are tabulated in Tables E.1 and E.2. The sources of these data are discussed in Sect. 2.

Table E.1. Data used in this work.

Source	l	b	E_{B-V}[a]	$\int \tau(\mathrm{HI})\, dv$[b]	$\int \tau(\mathrm{HCO^+})\, dv$[c]	W_{CO}[d]
	°	°	mag	km s^{-1}	km s^{-1}	K km s^{-1}
B1748-253	3.745	0.635	7.86	45.37(0.40)		
B2005+403	6.816	4.302	0.69	4.67(0.05)	0.41(0.02)	<0.20
B1730-130	12.032	10.812	0.53	10.91(0.17)	1.16(0.02)	0.47(0.12)
B1908-210	16.857	−13.219	0.28		<0.30	<0.20
B1819-131	17.910	0.372	7.99	63.71(1.00)		
B1817-098	20.711	2.293	1.55	20.62(0.49)		
B1819-096	21.047	1.957	3.08	29.01(0.40)		
B1829-106	21.347	−0.629	11.56	66.05(0.53)		
B1741-038	21.591	13.128	0.58	8.20(0.11)	1.11(0.10)	1.11(0.07)
B1849+005	33.498	0.194	16.93	117.62(0.87)		
B1749+096	34.920	17.644	0.09		<0.14	<0.20
B1909+049	39.694	−2.244	2.51	19.23(0.22)		
B1910+052	40.100	−2.336	2.10	17.68(0.41)		
B1843+098	41.112	5.772	0.57	6.71(0.16)		
B1915+062	41.605	−2.928	1.43	12.78(0.27)		
B1909+161	49.658	2.907	1.54	15.98(0.33)		4.47(0.06)
B1905+190	52.496	5.591	0.66	9.69(0.23)		
B1923+210	55.557	2.264	1.87	21.01(0.28)	2.28(0.12)	2.66(0.07)
B1950+253	62.366	−0.956	3.15	29.38(0.33)		
B1901+319	63.029	11.757	0.12	0.42(0.10)		
B1641+399	63.455	40.948	0.04		<0.09	<0.20
B2145+067	63.656	−34.072	0.08	0.98(0.02)	0.23(0.07)	<0.20
B2007+249	64.048	−4.334	1.27	14.12(0.21)		16.62(0.25)
J2023+319	71.397	−3.093	1.06	12.11(0.08)	1.55(0.04)	
B2015+33A	72.226	−0.978	3.48	46.23(0.34)		
B2015+33B	72.226	−0.981	3.48	37.55(0.43)		5.31(0.11)
B2023+336	73.129	−2.368	2.08	22.90(0.26)	3.43(0.02)	6.04(0.04)
B2048+313	74.585	−8.045	0.22	1.43(0.22)		
B2013+370	74.866	1.224	1.78	39.67(0.60)	3.12(0.02)	1.49(0.06)
B1954+513	85.298	11.757	0.15		1.68(0.06)	1.89(0.04)
B1823+568	85.739	26.080	0.06		<0.20	<0.20
B2251+158	86.111	−38.184	0.11	1.78(0.01)	0.30(0.01)	0.91(0.04)
B2037+511	88.808	6.040	1.02	17.32(0.13)	0.65(0.17)	0.51(0.06)
B2022+542	90.093	9.665	0.35	4.17(0.16)		
B2055+508	90.378	3.533	2.95	36.22(0.83)		19.65(0.12)
B2106+494	90.528	1.305	2.97	54.15(0.52)		15.53(0.09)
B2030+547	91.129	8.988	0.38	3.73(0.20)		
B2200+420	92.590	−10.441	0.33	3.74(0.04)	2.36(0.03)	6.78(0.05)
B2154+483	95.584	−4.860	0.53	7.51(0.13)		
B2111+620	100.287	9.429	0.84	10.72(0.18)		
B2146+608	102.570	5.713	0.85	11.04(0.11)		
B2201+62S	104.940	5.833	0.73	9.44(0.14)		
B1928+738	105.625	23.541	0.13		0.73(0.03)	<0.20
B2341+535	112.952	−7.745	0.33	5.62(0.09)		
B2255+702	113.596	9.707	0.52	5.27(0.10)		
B2357+554	115.718	−6.503	0.31	4.65(0.23)		
B2357+55B	115.719	−6.498	0.31	2.27(1.10)		
B2348+644	116.513	2.555	1.26	31.56(0.17)		
B0012+610	118.548	−1.264	1.65	34.20(0.15)		0.59(0.06)
B0016+731	120.644	10.728	0.32	1.99(0.14)		
B0041+660	122.253	3.449	2.18	44.63(0.32)		25.80(0.11)
B0052+681	123.351	5.503	1.00	10.79(0.06)		

Notes. [a] Reddening from Schlegel et al. (1998) rms error is 16%; [b] $\int \tau(\mathrm{HI})\, dv$ from Garwood & Dickey (1989) and (for J-sources) this work see Sect. 2; [c] $\int \tau(\mathrm{HCO^+})\, dv$ from Lucas & Liszt (1996), Liszt & Lucas (2000) and this work see Sect. 2; [d] W_{CO} from Lucas & Liszt (1996), Liszt & Lucas (1998) and this work see Sect. 2.

Table E.2. Data used in this work (continued).

Source	l	b	E_{B-V}[a]	$\int \tau(\mathrm{HI})\,dv$[b]	$\int \tau(\mathrm{HCO^+})\,dv$[c]	W_{CO}[d]
	°	°	mag	km s^{-1}	km s^{-1}	K km s^{-1}
B0056+666	123.782	3.992	1.20	13.30(1.05)		
J0102+584	124.426	−4.436	0.56	9.75(0.10)	0.34(0.01)	<0.34
B0107+562	125.637	−6.231	0.39	4.56(0.07)		
B0125+628	127.109	0.538	1.60	36.54(0.59)		6.81(0.09)
B0212+735	128.927	11.964	0.76	12.36(0.13)	4.98(0.20)	6.81(0.06)
B0205+614	132.064	0.210	1.55	27.59(0.45)		21.54(0.06)
B0224+671	132.122	6.234	1.00	14.73(0.24)	2.46(0.07)	2.27(0.06)
B0241+623	135.636	2.431	0.73	8.38(0.71)		
B0323+55A	143.890	−1.057	1.75	37.96(0.30)		
B0300+471	144.986	−9.863	0.25	4.99(0.14)		
B0954+658	145.746	43.132	0.12		1.23(0.29)	1.94(0.04)
B0332+534	145.952	−1.6810	1.68	31.89(0.35)		
B0334+506	147.809	−3.895	1.24	18.77(0.14)		
B0430+587	148.581	7.536	0.54	5.80(0.19)		
B0355+508	150.377	−1.604	1.50	42.79(1.10)	6.48(0.03)	16.82(0.12)
3C84	150.577	−13.261	0.05		<0.10	<0.20
B0442+506	155.877	3.460	0.94	13.14(0.21)		
B0435+487	156.417	1.317	1.35	27.84(0.22)		
B0235+164	156.772	−39.108	0.03		<0.20	<0.20
B0404+429	156.780	−6.586	0.49	11.73(0.13)		
B0420+417	159.705	−5.382	0.74	12.93(0.12)		
B0458+477	159.712	3.653	0.72	15.07(0.14)		
B0406+386	159.845	−9.484	1.02	12.12(0.12)		
B0429+416	160.965	−4.342	0.56	11.55(0.04)		
B0415+379	161.686	−8.788	1.66	12.14(0.14)	13.34(0.65)	17.45(0.11)
B0442+39A	164.109	−3.656	0.56	6.69(0.12)		
B0509+406	166.502	0.916	0.53	14.45(0.16)		
B0552+398	171.647	7.285	0.44	7.71(0.12)	0.69(0.08)	0.33(0.04)
B0923+392	183.709	46.165	0.10		<0.09	<0.20
B0601+204	189.566	−0.640	1.37	33.58(0.56)		
B0528+134	191.368	−11.012	0.89	11.88(0.20)	2.14(0.02)	2.53(0.06)
B0629+160	196.582	3.204	0.46	7.54(0.25)		
B0622+147	196.983	1.103	0.82	26.07(0.46)		
B0629+104	201.531	0.508	1.81	27.96(0.25)		
B0630+082	203.544	−0.272	0.91	28.65(0.33)		
B0624-058	215.439	−8.067	0.71	5.55(0.02)		
J0008+686	215.752	−13.253	1.28		7.16(0.75)	13.79(0.05)
B0605-085	215.752	−13.523	0.58		2.17(0.25)	1.31(0.13)
B0736+017	216.990	11.380	0.13	2.96(0.17)	0.89(0.10)	0.92(0.04)
B0607-157	222.611	−16.183	0.26		0.36(0.09)	<0.20
B0727-115	227.768	3.140	0.30	6.81(0.14)	0.55(0.02)	0.81(0.04)
B0733-174	233.585	1.444	0.92	20.00(0.13)		
B0709-206	233.670	−5.021	0.98	19.22(0.28)		
B0704-231	235.337	−7.218	0.33	7.28(0.10)		
B1055+018	251.513	52.775	0.20		<0.24	<0.20
3C273	289.954	64.360	0.03		<0.08	<0.20
3C279	305.107	57.062	0.05		<0.07	<0.20
B1334-127	320.026	48.374	0.04		<0.17	<0.20
B1714-397	347.748	−1.142	3.53	39.45(0.20)		
B1705-353	350.339	2.768	1.74	21.39(1.30)		
B1714-336	352.735	2.393	2.42	29.58(0.88)		
B1711-285	356.516	5.884	0.60	8.64(0.27)		

Notes. [a] Reddening from Schlegel et al. (1998) rms error is 16%; [b] $\int \tau(\mathrm{HI})\,dv$ from Garwood & Dickey (1989) and (for J-sources) this work see Sect. 2; [c] $\int \tau(\mathrm{HCO^+})\,dv$ from Lucas & Liszt (1996), Liszt & Lucas (2000) and this work see Sect. 2; [d] W_{CO} from Lucas & Liszt (1996), Liszt & Lucas (1998) and this work see Sect. 2.